ChemElectroChem

Research Article
doi.org/10.1002/celc.202200100

Chemistry Europe
European Chemical Societies Publishing

www.chemelectrochem.org

Special Collection

Effect of Thermal Treatment on Nickel-Cobalt Electrocatalysts for Glycerol Oxidation

Teresa Andreu,*[a] Maria Mallafré,[a] Martí Molera,[a] Maria Sarret,[a] Roger Oriol,[b] and Ignasi Sirés[b]

Nickel-cobalt electrocatalysts with atomic ratios of 2:1 and 1:2 were synthesized on nickel foam (NF) substrates by cathodic electrodeposition, further evaluating the performance of the pristine and thermally-treated materials as anodes for glycerol oxidation in alkaline medium. The electrodes were characterized by cyclic and linear sweep voltammetry at alkaline pH, showing an indirect oxidation of glycerol mediated by the metal oxyhydroxides. Under the selected conditions, a favourable potential window of 0.2 V upon comparison of water and glycerol oxidation was found. In addition, the increase in nickel content and the thermal treatment enhanced the anode polarization. After galvanostatic electrolysis at 10 mA cm^{-2}, the products were analysed by HPLC, formate ion being the primary product, with a faradaic efficiency (FE) higher than 70% in most cases. Both the FE to formate and the glycerol conversion were substantially enhanced using the thermally-treated anodes, whereas the effect of the Ni/Co ratio on these two parameters did not follow a clear trend.

Introduction

In the present and upcoming highly electrified energy scenarios, electrolysis technologies are gaining momentum. In particular, electrochemical hydrogen production in devices that promote either water or carbon dioxide electroreduction is becoming a key technology to achieve climate neutrality. For this kind of electrolyses, recent studies have pointed out the need to replace the sluggish anodic oxygen evolution reaction (OER) by alternative reactions that allow reducing the required overpotential that currently limits their economic feasibility.[1,2] To this end, the oxidation of biomass-derived alcohol is foreseen as an interesting approach, since alcohols can be partially oxidized to value-added products and, in case of complete mineralization, their associated CO_2 emissions are considered neutral.

The surplus of crude glycerol formed as by-product in the biodiesel industry (100 kg glycerol per ton of biodiesel) has made this chemical highly available at a low commercial price, thereby increasing the interest on its catalytic valorization. Among the most promising upgrading routes, electrocatalysis constitutes an emerging field,[3] as recently exemplified employing water or CO_2 co-electrolyser.[4,5]

Most of the studies on the electrochemical glycerol oxidation reaction (GOR) with non-noble metal catalysts in alkaline media have been focused on nickel- and cobalt-based oxides, hydroxides or oxyhydroxides,[6,7] owing to the earth abundance, relatively low price and mild toxicity of Ni and Co as transition metals.[8] The best established mechanism for GOR is based on the indirect alcohol oxidation mediated by M^{II},[9,10] although a clear elucidation of the preferred Ni–Co structure has not been provided yet. Han et al. proposed $CuCo_2O_4$ and $NiCo_2O_4$ spinel oxides as GOR electrocatalysts with a high faradaic efficiency (FE) to formic acid, being the catalysts synthetized by hydrothermal treatment to obtain a layered double hydroxide (LDH) that was subsequently annealed at 300 °C to induce its transformation into the oxide form.[11] In contrast, Deng et al. described the direct use of a Ni–Co LDH or metal-organic framework (MOF) with the sole electrochemical activation by successive cycling.[12]

In this context, the aim of this work is to discern whether the raw hydroxide or the promoted oxide form of a Ni–Co LDH as precursor of a spinel structure is the most suitable electrocatalyst for glycerol oxidation in alkaline medium. Being the general formula of a spinel $M^{II}M^{III}{}_2O_4$, Ni foam (NF)-supported materials with Ni/Co atomic ratios of 2:1 and 1:2 were synthetized by electrodeposition, since this method has been demonstrated to induce a superior electrocatalytic activity as compared to the hydrothermal synthesis.[13]

[a] Prof. T. Andreu, M. Mallafré, M. Molera, Prof. M. Sarret
Sustainable Electrochemical Processes. Department of Materials Science and Physical Chemistry & Institute of Nanoscience and Nanotechnology (IN^{2}UB).
Facultat de Química, Universitat de Barcelona
Martí i Franquès, 1-11, 08028 Barcelona, Spain
E-mail: tandreu@ub.edu

[b] R. Oriol, Prof. I. Sirés
Laboratori d'Electroquímica dels Materials i del Medi Ambient
Departament de Química Física.
Facultat de Química, Universitat de Barcelona
Martí i Franquès 1-11,08028 Barcelona, Spain

Supporting information for this article is available on the WWW under https://doi.org/10.1002/celc.202200100

Special Collection An invited contribution to a Special Collection on Current Trends in Electrochemistry 2021 for the 1st French-Spanish Workshop on Electrochemistry

Results and Discussion

Ni–Co electrocatalysts with atomic ratios of 2:1 and 1:2 were synthesized on NF electrodes by nitrate-assisted electrodeposition from the metal sulfate precursors. Under cathodic polarization, nitrate was reduced to ammonia, simultaneously creating an alkaline environment at the vicinity of the cathode surface that caused the co-precipitation of cobalt and nickel hydroxides. Due to the inherent redox activity of both metal centers, which may arise from the M^{III}/M^{II} interconversion, it is highly probable that the electrical neutrality of the final mixed hydroxide can only be ensured by facilitating water and counterion intercalation, eventually balancing the charges and creating layered structures (i.e., LDHs). After 15 min of electrodeposition, an average mass loading of 13 ± 1 mg cm^{-2} was obtained for 2:1 Ni/Co ratio, whereas 10 ± 1 mg cm^{-2} resulted in the case of 1:2 Ni/Co ratio. This informs about a less efficient process in the latter case, in agreement with the different solubility product constants (K_{sp}) at 25 °C of $Co(OH)_2$ ($5.92 \cdot 10^{-15}$) and $Ni(OH)_2$ ($5.48 \cdot 10^{-16}$).[14] Once subjected to thermal treatment (TT), a mass loss of around 3 mg cm^{-2} was observed in all cases, attributed to dehydration and dehydroxylation processes.[15]

Surface characterization

A selection of the SEM images of the four different samples can be seen in Figure 1. The surface composition of the four samples was analyzed by EDX and as can be noted in Figure S1 in Supplementary Information (SI), a good agreement between the expected Ni/Co ratios and those determined experimentally was obtained, although an excess or deficit of Ni or Co can be noticed in some spots. In all regions, the elemental analysis showed the presence of sulfur element in the deposits (Figure S2 in SI), which can be accounted for by the intercalation of sulfate ions within the structure. This corroborates the formation of the layered double hydroxides regardless of the bath composition. Besides sulfate, other counterions like nitrate can be presumed to become intercalated as well, in agreement with the electrolyte composition, although their presence cannot be ascertained categorically (Figure S2). In all samples, FT-IR spectra (Figure S3) show a broad peak with two contributions at 1110 and 1060 cm^{-1} corresponding to the asymmetric and symmetric stretching modes of S–O bonds of intercalated sulfate ions.[16] In addition, the characteristic stretching vibrations of interlayer water molecules and nitrate ions were found at 1630 cm^{-1} and 1384 cm^{-1}, respectively, corroborating the formation of a layered structure.[17]

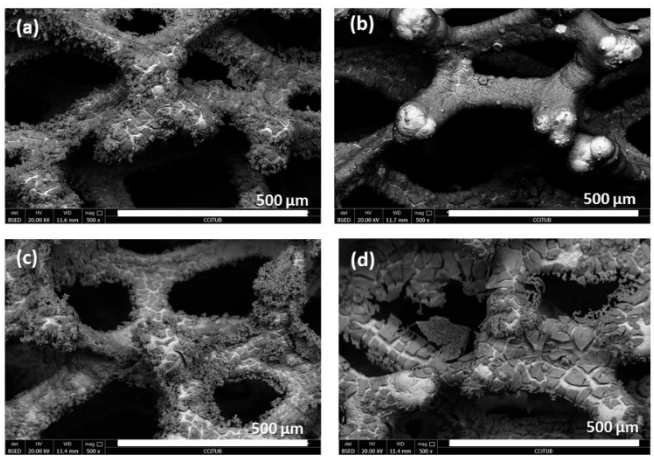

Figure 1. SEM images of samples with Ni/Co atomic ratios of 2:1 (a), 2:1-TT (b), 1:2 (c) and 1:2-TT (d). TT refers to thermally-treated samples

In the SEM micrographies, the deposits clearly reveal two distinctive morphologies. On the one hand, a characteristic porous and laminar LDH structure that preserves the Ni/Co atomic ratio of the electrodeposition solution can be distinguished. This structure was more typically found near the edges of the coating. On the other hand, a more compact structure is also present, showing a preferential deposition of cobalt (i.e., deficit of nickel *vs.* electrolyte composition). In fact, the compact structure was the predominant one as the cobalt concentration in the electrolyte was increased. Considering that cobalt cations may have a higher water coordination number than nickel cations, cobalt can reach the inner Helmholtz layer more easily than nickel cations. Indeed, it has been reported that $CoOH^+/Co(OH)_2$ have higher adsorption tendency as compared to $NiOH^+/Ni(OH)_2$, being one of the plausible mechanisms of the anomalous deposition.[18]

XPS analysis was performed to corroborate the chemical structure of the materials. As shown in Figure S4, the Ni 2p spectrum presents a doublet at 873.5 eV ($2p_{1/2}$) and 855.8 eV ($2p_{3/2}$) with two satellite peaks, accounting for the presence of Ni(II). The Co 2p region presents the spin-orbit splitting located at 796.7 eV and 781 eV, together with two less intense satellite peaks, in agreement with the coexistence of Co(II) and Co(III).[19] The S 2p peak is a broad band centered at 168.7 eV, attributed to sulfate ions.[20] Finally, the O 1s peak presents two distinctive features; all the samples have a contribution centered at 531.5 eV corresponding to metal hydroxides and, moreover, the samples that were subjected to the thermal treatment exhibit a second intense band related to M–O–M bonds located at 529.8 eV.[17] This can be explained by the dehydration and the subsequent partial dehydroxylation reaction, preferentially yielding the oxide forms,[21] which was corroborated by the shift on the XRD patterns (Figure S5) for the thermally-treated samples. Despite their low crystallinity, pristine samples can be indexed to nickel-based LDH (JCPDS 38-0715), which was partially transformed to nickel oxide phases (JCPDS 22-1189) or nickel cobaltite (JCPDS 20-0781).

Voltammetric study

The electrocatalytic properties of 2:1 and 1:2 Ni/Co catalysts were first investigated using cyclic voltammetry in alkaline electrolyte (1 M KOH) in the absence (Figure 2a) and the presence of 0.1 M glycerol (Figure 2b). All curves in Figure 2 correspond to the tenth cycle once the surface is stabilized. As

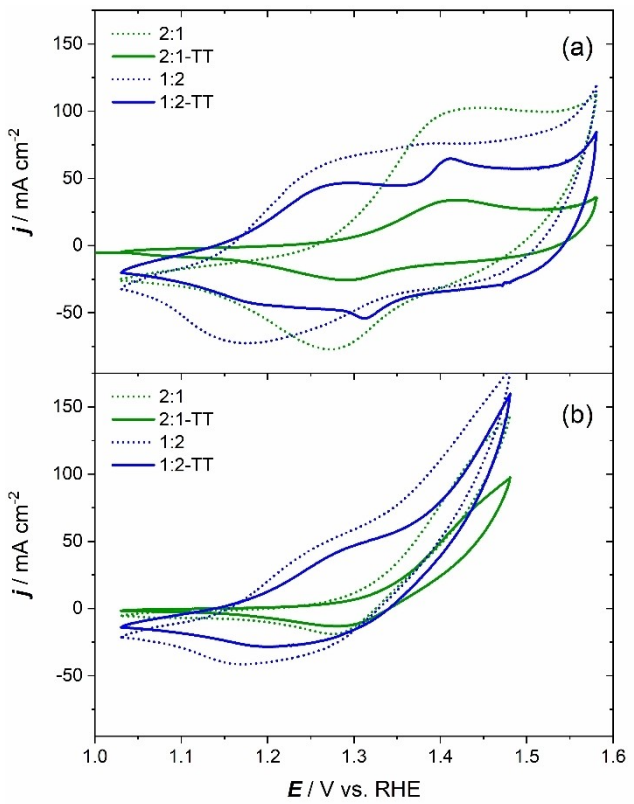

Figure 2. Cyclic voltammograms obtained for the electrodes with Ni/Co ratio of 2:1 (green) and 1:2 (blue) in 1 M KOH electrolyte (a) and 1 M KOH + 0.1 M glycerol electrolyte (b). TT refers to thermally-treated samples (solid lines) Scan rate: 20 mV s^{-1}.

can be seen in Figure S6, as compared with the first cycle, during the initial voltametric cycles (i.e., cycles 2–10) in the absence of glycerol, the areas of peaks attributed to the M^{III}/M^{II} (M=Ni, Co) interconversion for the as-prepared hydroxides tended to become slightly reduced. Conversely, the areas increased upon cycling for the thermally-treated ones, which is more evident in the case of the nickel-rich electrode (2:1-TT), attributed to the hydration of the oxide layers.[22] Regarding the first anodic scan, it showed a particular behavior, since in most cases the peak area was higher due to the surface and bulk oxidation of M^{II} to M^{III} (Figure S6), whereas in the subsequent cycles the electrochemically active M^{II} centers are mainly the ones previously reduced during the cathodic scan.

As shown in Figure 2a, the voltammograms evidenced two broad pairs of redox peaks in 1 M KOH electrolyte, which can be attributed to the hydroxide/oxyhydroxide electrochemical cycling (i.e., $M(OH)_2$/MOOH, with M=Ni, Co, Eq. 1) followed in the anodic scan by water oxidation with an onset potential in the range of 1.55–1.60 V_{RHE}. The anodic redox peaks of the nickel-rich samples (2:1 and 2:1-TT) were closer to the oxidation of $Ni(OH)_2$ to NiOOH at 1.42 V_{RHE} whereas for the cobalt-rich ones, an additional anodic peak centered at 1.25 V_{RHE} and plausibly attributed to the oxidation of $Co(OH)_2$ to CoOOH can be noticed.[23] After heat treatment, the oxidation peaks became narrower, which is particularly evident for the 1:2 ratio (Figure 2a); this occurred without a significant change in their peak potentials, resulting in a positive shift of the oxidation potentials in the range of 10 to 30 mA cm^{-2}. On the other hand, regardless of the electrode composition, the relative peak areas decreased with the heat treatment, due to the partial reorganization of the layered double hydroxide that caused a reduction of the electrochemically active surface area.

When glycerol was present in the alkaline electrolyte (Figure 2b), the polarization curve profiles overlapped with those of Figure 2a, thus yielding the same onset oxidation potentials. This finding corroborates that the ubiquitous preliminary step is the oxidation of M^{II} to M^{III} (Eq. 1). This transformation occurred in concomitance with the glycerol oxidation mediated by the generated metal oxyhydroxide, regenerating the $M(OH)_2$ according to Eq. 2. The $M(OH)_2$ production in the anodic scan can be confirmed from the resulting smaller area (as compared to those of Figure 2a) found in all cases during the cathodic scans, which resulted from the substantial reduction of M^{III} as glycerol became oxidized. Moreover, the occurrence of GOR impeded to distinguish the two distinct oxidation peaks observed for the 1:2-TT sample in 1 M KOH. At higher potentials, the aldehydes formed from Eq. 2 could be further oxidized to carboxylates (Eq. 3). To sum up, the cyclic voltammetry suggested that the glycerol oxidation occurred via the indirect alcohol oxidation mechanism, involving the three mentioned initial elementary steps.[7]

$$M(OH)_2 + OH^- \rightarrow MOOH + H_2O + e^- \quad (1)$$

$$MOOH + RCH_2OH + OH^- \rightarrow M(OH)_2 + H_2O + RCHO + e^- \quad (2)$$

$$RCHO + 3OH^- \rightarrow RCOO^- + 2H_2O + 2e^- \quad (3)$$

Figure 3 shows the linear sweep voltammograms obtained with all the electrodes, with the aim to compare the potential

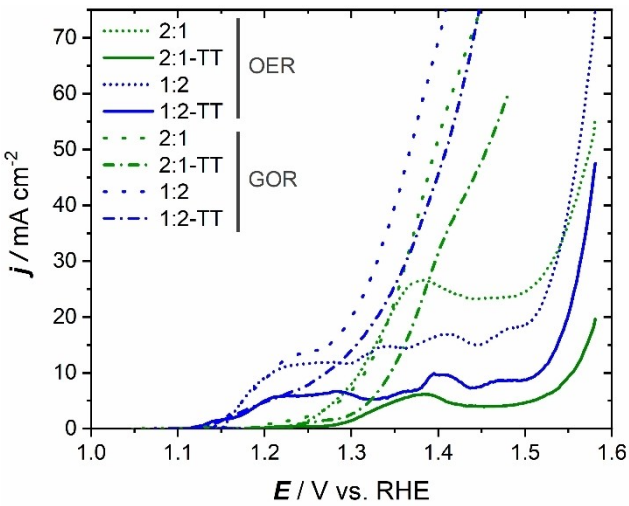

Figure 3. Linear sweep voltammograms (LSV) for the electrodes with Ni/Co ratio of 2:1 (green) and 1:2 (blue) in 1 M KOH electrolyte (OER) and 1 M KOH + 0.1 M glycerol electrolyte (GOR). TT refers to thermally-treated samples (solid lines) Scan rate: 2 mV s^{-1}.

window between glycerol and water oxidation reactions. In agreement with the cyclic voltammetry just described, for a given Ni/Co ratio, the onset oxidation potential was exactly the same regardless of the electrolyte and the electrodeposition post-treatment, since for all materials the current rise from zero was related to the hydroxide oxidation (Eq. 1). In particular, the onset was found at 1.15 V_{RHE} for the cobalt-rich electrodes (1:2 and 1:2-TT), whereas it was shifted to a more positive value in the case of nickel-rich electrodes (2:1 and 2:1-TT), around 1.25 V_{RHE}. In contrast, there was a significant difference between GOR and OER; the oxygen evolution reaction showed an onset potential around 1.50 V_{RHE}, being significantly higher than that of GOR occurring between 1.25 and 1.30 V_{RHE}. In general terms, all the thermally-treated electrocatalysts present a shift of their polarization curves towards anodic potentials, despite the *iR* correction.

According to the polarization curves of Figure 3, the cobalt-rich electrodes (1:2) have a higher glycerol electrooxidation activity as compared to the nickel-rich ones (2:1).

As mentioned in the introduction section, owing to its large availability as a by-product in industry, crude glycerol can be a potential electron donor for electrolytic hydrogen production, thereby becoming a nice solution to avoid the kinetically limited OER reaction that is still the state of the art in the field. Based on the LSV data, Table 1 offers an estimation of the electrode potentials for GOR and OER processes, as well as of the energy savings considering an atmospheric alkaline electrolyser operating at room temperature and 25 mA cm^{-2}. The electrode potential difference to carry out both reactions was around 0.2 V, resulting in an energy saving close or even higher than 5 kWh kg_{H2}^{-1}. This would result in an increase of 12–15% in the energy efficiency of the electrolysis process, taking into account the HHV or LHV values of hydrogen (i.e., 39.4 and 33.3 kWh kg_{H2}^{-1}, respectively). A more comprehensive analysis considering energy and mass balances should be done to fully assess the economic viability, but this first calculation allows being optimistic.

Table 1. Electrode potentials and energy savings from LSV data at 25 mA cm^{-2}.

Sample	E_{GOR}/V_{RHE}	E_{OER}/V_{RHE}	ΔE/[mV][a]	ES/[kWh kg_{H2}^{-1}][b]
2:1	1.35	1.51	160	4.29
2:1-TT	1.38	1.58	200	5.36
1:2	1.31	1.52	210	5.63
1:2-TT	1.35	1.55	200	5.36

[a] Electrode potential difference: E_{OER}–E_{GOR}. [b] Energy saving calculated from ΔE (Eq. S1 in section 6 of SI).

Galvanostatic oxidation of glycerol

Glycerol can be oxidized to a wide variety of products (see SI, section 7) in alkaline media, involving a different number of hydroxide ions and electron stoichiometries. As described in Eq. 2, the general electrooxidation mechanism involves the formation of a carbonyl group, which can occur in the central or terminal position being dihydroxyacetone or glyceraldehyde, respectively, the first intermediates. In alkaline media, the latter is the most stable species, and it can be successively oxidized to glycerate and C1–C2 products such as formate, glycolate and oxalate ions. To elucidate the selectivity and faradaic efficiency of the process, a galvanostatic electrolysis was performed at 10 mA cm^{-2}, a current value that is considered as representative in the design of solar-powered water splitting devices.[24]

Three consecutive electrolytic trials were carried out, at accumulated charges of 7.5, 15 and 30 C mL^{-1}. As a result of the electrolysis, as summarized in Table 2, formate ion was the compound accounting for the highest FE. This FE was in most cases higher than 70% and, in the case of the thermally-treated samples, the efficiency to formate increased by 4%-10%. Besides formate, as determined by HPLC analysis (Figure S7), oxalate and glycolate were also formed. These were accompanied by unquantified products, with major predominance of ketomalonate (route A in Figure 4), since 1,3-dihydroxyacetone and its subsequent oxidation products were much less abundant (route B in Figure 4). Note that the FE sum of both oxalate and glycolate was always below 10%. Considering the ratio of their FE with the sum of C1–C2 products, as the electrolysis progressed, the tendency in all samples was to decrease the ratio of glycolate in favor of oxalate. The later was a more oxidized product (Figure 4) whose formation was favored by

Table 2. Summary of the glycerol conversion and faradaic efficiencies for glycerol oxidation at 10 mA cm^{-2}. Electrolyte: 1 M KOH + 0.1 M glycerol.

Sample	Charge passed [C mL^{-1}]	Glycerol conversion [%]	Faradaic efficiency [%][a] Formate	Oxalate	Glycolate	Σ[b]
2:1	7.5	11.1	74.1	4.4	4.5	83.0
	15	19.5	71.6	4.4	3.8	79.8
	30	34.3	67.3	5.3	3.0	75.6
2:1-TT	7.5	14.6	79.4	4.1	5.5	89.0
	15	26.6	77.3	4.3	4.5	86.0
	30	41.5	75.0	4.4	3.7	83.0
1:2	7.5	7.6	71.0	3.6	5.2	79.9
	15	14.2	73.2	3.7	5.7	82.6
	30	31.0	70.9	3.6	4.7	79.2
1:2-TT	7.5	14.1	80.6	3.0	4.8	88.4
	15	26.8	76.9	3.2	3.9	84.0
	30	42.3	74.9	2.8	3.3	81.0

[a] Calculated from HPLC analysis. [b] Sum of C1–C2 faradaic efficiencies to formate, oxalate, and glycerate.

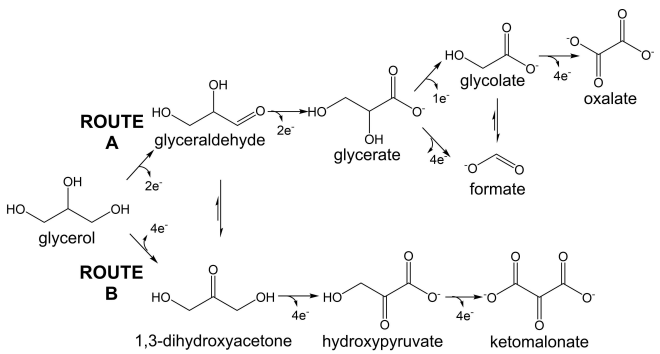

Figure 4. Scheme of possible oxidation routes in alkaline media.

the increased electrode potential monitored as shown in Figure 5.

Regarding the glycerol conversion, the values with the as-prepared hydroxides were always lower than the glycerol conversions attained with the thermally-treated ones (Table 2).

The fact that in the case of the pristine LDH electrodes the FE to formate ions was always lower than that reached using the calcined samples is in good agreement with the potential difference between the as-prepared and thermally-treated electrocatalysts. The higher the electrode polarization, as occurred in the case of TT samples (Figure 3 and Table 1), the higher the FE to highly oxidized products (C1). Conversely, the lower glycerol conversion values observed in the as-prepared hydroxides suggests that the unquantified products correspond to oxidation compounds whose formation involves a higher number of electrons, such as ketomalonate ions that requires 10 electrons. This was verified from HPLC analysis, since despite the inaccuracy due to the peak overlapping (Figure S7), a rough estimation yielded around 10% of ketomalonate. Note that this was the only product detected from route B, which confirms the prevalence of route A. Considering that the total organic carbon of the electrolyte employed in these trials remained constant over the electrolysis, which excludes the possibility of glycerol mineralization to CO_2, and that the electrode potential was below that required for the competitive oxygen evolution reaction, the most plausible hypothesis is the occurrence of change in the oxidation mechanism between when comparing both types of samples.

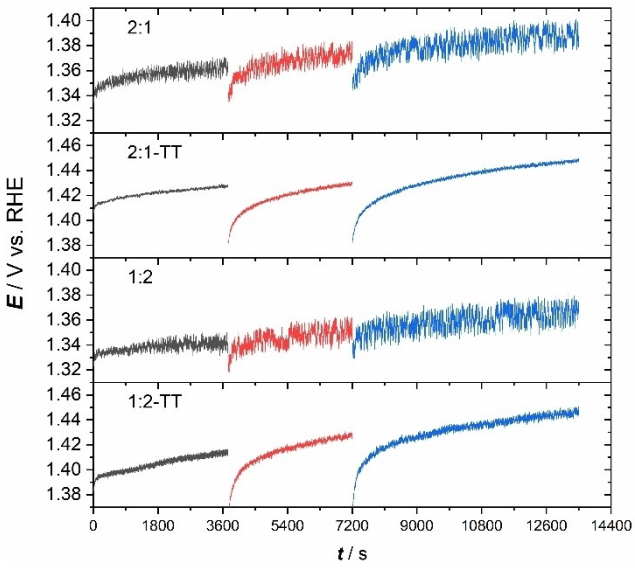

Figure 5. Chronopotentiometric curves made during the consecutive electrolysis at 10 mA cm^{-2}. At the end of each period, the accumulated charge was 7.5, 15 and 30 C mL^{-1}, respectively. Electrolyte: 1 M KOH + 0.1 M glycerol. The electrode potential was recorded without *iR* compensation.

The chronopotentiometry recorded during the electrolysis under galvanostatic conditions allowed the monitoring of the anode potential, as shown in Figure 5. Despite the general tendency in all the electrodes to undergo a potential increase as the reaction progressed, which agrees with the Nernst equation (i.e., the glycerol was gradually oxidized), two distinctive behaviors can be readily observed, depending on the electrodeposition post-treatment.

The electrode potential of hydroxide samples showed a signal perturbation, which became more remarkable with the accumulated charge rising from 7.5 to 30 C mL^{-1}. This oscillating perturbation was already reported for static platinum electrodes subjected to constant current for the oxidation of C1–C3 compounds such as glycerol, in both alkaline and acidic media.[25] However, it was not reported before for nickel- or cobalt-based electrocatalysts. In the present case, the oscillation frequencies and amplitudes were significantly lower than those observed for platinum rotating disc electrodes, which can be in the order of 50–200 mV in KOH electrolytes.[26] As depicted in Figure S8, the potential oscillated with a peak-to-peak amplitude from 8 to 20 mV and frequencies ranging from 0.025 to 0.01 Hz. Usually, potential oscillations are attributed to a poisoning mechanism or mass transport issues. However, a recent study suggested that besides insufficient mass transport, the electrode potential instability can be related to the double-route mechanism involving the commutation between the dihydroxyacetone and glyceraldehyde reaction intermediates (Figure 4) by glycerol products re-adsorption.[27] In our case, it implies that the glyceraldehyde route is partially restricted when using the pristine electrocatalysts, leading to lower formate yields, favouring the dihydroxyacetone route that preferentially leads to the highly oxidized C3 compound ketomalonate ion (in agreement with the comments made above). A previous study on gold electrodes in alkaline media demonstrates the role of hydroxyl adsorption in modifying the re-adsorption of oxidized glycerol intermediates,[28] which can be extended to the native hydroxides of the untreated samples as compared to the TT ones.

Regarding the effect of the Ni/Co ratio, no significant differences were observed for the glycerol conversion and C1–C2 faradaic efficiencies, except that for the cobalt-rich samples (1:2) the ratio of oxalate and glycerate with the sum of C1–C2 products was slightly smaller than that determined for the nickel-rich samples (2:1), in agreement with the lower electrode potentials recorded (see previous comments on the LSV results).

As a summary, when both Ni and Co metals are present in the anode, there is only a small impact of their relative percentage on the reaction mechanism, which is much more sensitive to the thermal treatment. Besides, in agreement with recent studies that suggest the possible catalytic role of sulfate, its effect could be discussed in future works.[29,30]

Conclusion

Ni/Co electrocatalysts with atomic ratios of 2:1 and 1:2 were synthesized on NF cathodes, the ensembles further being employed as untreated or thermally-treated anodes for glycerol oxidation in alkaline medium, with the aim to elucidate the effect of both the Ni/Co ratio and the calcination. The catalysts were synthesized by electrodeposition from a nitrate-sulfate electrolyte that allowed obtaining two different LDHs, whose thermal treatment at 300 °C caused a mass loss attributed to the removal of compensating anions present in the LDHs. The two untreated and two thermally-treated electrodes were characterized by cyclic voltammetry and linear sweep voltammetry in alkaline medium, in the presence and absence of glycerol. The results showed that in these two cases, the onset potential for the metal hydroxide electrocatalyst oxidation was the same. Regarding the GOR, it was mediated by the resulting oxyhydroxide, and the presence of a greater nickel content as well as the application of the thermal treatment led to a higher anode polarization, which is detrimental in terms of energy need. A potential difference of 0.2 V was determined when comparing the water and glycerol oxidation voltammograms at 25 mA cm^{-2}, which may exert a positive impact of up to 15% on the energy requirement for electrolytic hydrogen production. Galvanostatic electrolytic trials showed that formate ion was the primary product, with an FE often higher than 70%. It was found that the hydroxide samples suffer from electrode potential oscillations that may restrict the glycerol conversion. Thermally-treated coatings appeared to show higher stability upon repeated usage, although the actual long-term stability should be studied with more detail in a focused work. Regarding the Ni/Co ratio, the best proportion has not been clearly elucidated but, in all cases, the TT had a more relevant role as it improved the FE to formate as well as the overall glycerol conversion.

Experimental Section

Ni–Co electrodes were prepared by cathodic electrodeposition on nickel foam (NF) substrates (Recemat Ni-4753, 1.6 mm thick, 1 × 3 cm^2 with immersed geometric area of 1.5–2 cm^2) pre-cleaned with HCl 2 M to remove the native oxides. The electrolyte was an aqueous solution (70 mL) of 0.1 M $NaNO_3$ and 0.1 M of metal precursors ($NiSO_4 \cdot 6H_2O$ and $CoSO_4 \cdot 7H_2O$) with the desired Ni/Co ratio (2:1 or 1:2). The electrosynthesis process was based on the nitrate anion reduction reaction at −1.0 V vs Ag|AgCl (3.5 M KCl) (Methrom) that simultaneously causes the precipitation of nickel and cobalt hydroxides.[31] Pt wire (0.5 mm diameter, Heraeus) was used as counter electrode. The potentiostatic deposition was carried out at room temperature for 15 min using a VMP-2 Biologic multichannel potentiostat. Some of the samples were then subjected to a thermal treatment (TT) at 300 °C for 2 h in air atmosphere. At least two batches of untreated and thermally-treated samples were prepared, in order to confirm the reproducibility of all results. The morphology and the composition of the electrodes were verified by using a Quanta 200 SEM microscope with an energy dispersive X-ray spectroscopy (EDS) detector. Fourier transformed infrared (FT-IR) spectra was recorded using an attenuated total reflectance (ATR) FT-IR instrument Spectrum Two from Perkin Elmer. X-ray photoelectron spectroscopy (XPS) experiments were performed in a PHI 5500 Multitechnique System (from Physical Electronics) with a monochromatic X-ray source (Al K_α 1486.6 eV). X-ray diffraction (XRD) analysis was performed using a PANalytical X'Pert PRO MPD Alpha1 powder diffractometer with Fe filtered Co Kα radiation (λ = 1.789 Å) working at 45 kV–40 mA in a Bragg Brentano configuration.

The electrochemical evaluation referred to the oxygen evolution reaction (OER) and glycerol oxidation reaction (GOR) was carried out using the same potentiostat or a VSP300 model. This characterization was made in a 3-electrode electrochemical cell comprising one of the untreated or thermally-treated samples as working electrode (exposed geometric electrode area of 1 cm^2, delimited with Teflon tape), as well as a platinum and a double junction Ag|AgCl (3.5 M KCl) as counter and reference electrodes, respectively. For CV and LSV techniques, the electrode potential was corrected with 80% of ohmic drop compensation. The electrolyte employed (70 mL) was 1 M KOH for OER studies and 1 M KOH + 0.1 M glycerol for GOR. All potentials have been converted to the reversible hydrogen reference electrode (RHE) using the Nernst equation, considering $E^0 = 0.205\ V_{RHE}$ at 25 °C.

To determine the faradaic efficiency for glycerol oxidation, the experiments were carried out in a single compartment electrochemical cell with only 5 mL capacity to concentrate the products for the subsequent analysis by HPLC. The electrolyte solution contained 1 M KOH + 0.1 M glycerol. Electrolysis experiments were carried out under galvanostatic conditions (10 mA cm^{-2}) and the anode potential was measured using a 1 mm leak-free Ag|AgCl (3.4 M KCl) reference electrode (Warner Instruments). Two aliquots (i.e., replicates) of 200 μL were taken for analysis at each given interval (7.5, 15 and 30 C mL^{-1}). Samples were immediately acidified by adding 600 μL of 0.167 M H_2SO_4. The oxidation products were analysed by high-performance liquid chromatography (HPLC) with an Alliance e2695 separation module (Waters) as management platform, with a sample loop of 100 μL and an ion exclusion column (Aminex HPX-87H, BioRad) at 60 °C. Diluted sulfuric acid (10 mM H_2SO_4) was used as eluent with a flow rate of 0.6 mL·min^{-1}. The chromatograph was equipped with an UV/Vis detector (Jasco UV-1570) selected at 210 nm and a refractive index detector (RID, Waters 2414) thermostated at 35 °C. The main peak corresponded to formate, whose peak appeared at 14.1 min, being accompanied by less intense peaks related to oxalate, glycerate and ketomalonate.

Acknowledgements

This work was funded by MCIN/AEI/10.13039/501100011033 projects PID2019-108136RB-C33 and PID2019-109291RB-I00. The authors also thank the support from Generalitat de Catalunya through the 2017SGR100 and 2017SGR1777 projects. R. Oriol acknowledges the FPI grant BES-2017-080095 awarded by MINECO (Spain). The authors acknowledge the contribution of Simon

Prueflinger during his Erasmus internship and Scientific and Technological Centers (CCiTUB).

Conflict of Interest

The authors declare no conflict of interest.

Data Availability Statement

The data that support the findings of this study are available from the corresponding author upon reasonable request.

Keywords: Electrocatalysis · Glycerol oxidation · Hydrogen production · Nickel-Cobalt catalyst · Thermal treatment

[1] S. Verma, B. Kim, H. R. M. Jhong, S. Ma, P. J. A. Kenis, *ChemSusChem* **2016**, *9*, 1972–1979.
[2] S. Verma, S. Lu, P. J. A. Kenis, *Nat. Energy* **2019**, *4*, 466–474.
[3] M. Checa, S. Nogales-Delgado, V. Montes, J. M. Encinar, *Catalysts* **2020**, *10*, 1–41.
[4] Y. Xu, M. Liu, S. Wang, K. Ren, M. Wang, Z. Wang, X. Li, L. Wang, H. Wang, *Appl. Catal. B: Environ.* **2021**, *298*, 120493.
[5] G. Wang, J. Chen, K. Li, J. Huang, Y. Huang, Y. Liu, X. Hu, B. Zhao, L. Yi, T. W. Jones, Z. Wen, *Nano Energy* **2022**, *92*, 106751.
[6] C. Coutanceau, S. Baranton, R. S. B. Kouamé, *Front. Chem.* **2019**, *7*, 100.
[7] T. Li, D. A. Harrington, *ChemSusChem* **2021**, *14*, 1472–1495.
[8] B. Su, Z. C. Cao, Z. J. Shi, *Acc. Chem. Res.* **2015**, *48*, 886–896.
[9] J. Kaulen, H. J. Schäfer, *Tetrahedron* **1982**, *38*, 3299–3308.
[10] M. Fleischmann, K. Korinek, D. Pletcher, *J. Electroanal. Chem. Interfacial Electrochem.* **1971**, *31*, 39–49.
[11] X. Han, H. Sheng, C. Yu, T. W. Walker, G. W. Huber, J. Qiu, S. Jin, *ACS Catal.* **2020**, *10*, 6741–6752.
[12] X. Deng, M. Li, Y. Fan, L. Wang, X. Z. Fu, J. L. Luo, *Appl. Catal. B: Environ.* **2020**, *278*, 119339.
[13] S. Zhuang, L. Wang, H. Hu, Y. Tang, Y. Chen, Y. Sun, H. Mo, X. Yang, P. Wan, Z. U. H. Khan, *ChemElectroChem* **2018**, *5*, 2577–2583.
[14] J. R. Rumble, ed., *CRC Handbook of Chemistry and Physics*, *102 Edition (Internet Version 2021)*, **2021**, CRC Press/Taylor & Francis, Boca Raton, FL.
[15] C. Hobbs, S. Jaskaniec, E. K. McCarthy, C. Downing, K. Opelt, K. Güth, A. Shmeliov, M. C. D. Mourad, K. Mandel, V. Nicolosi, *2D Mater.* **2018**, *2*, 1–10.
[16] A. Q. Wang, J. X. Wang, H. Wang, Y. N. Huang, M. L. Xu, X. L. Wu, *RSC Adv.* **2017**, *7*, 14224–14232.
[17] B. Xiao, W. Zhu, Z. Li, J. Zhu, X. Zhu, G. Pezzotti, *R. Soc. Open Sci.* **2018**, *5*, 180867.
[18] K. Kim, D. Raymond, R. Candeago, X. Su, *Nat. Commun.* **2021**, *12*, 1–10.
[19] A. Tang, P. Chen, C. Mi, *Ionics* **2020**, *26*, 6277–6287.
[20] Y. Wang, Z. Yin, G. Yan, Z. Wang, X. Li, H. Guo, J. Wang, *Electrochim. Acta* **2020**, *336*, 135734.
[21] C. S. de Matos, C. M. Ghimbeu, J. Brendlé, L. Limousy, V. R. L. Constantino, *New J. Chem.* **2020**, *44*, 16721–16732.
[22] S. Corby, M. G. Tecedor, S. Tengeler, C. Steinert, B. Moss, C. A. Mesa, H. F. Heiba, A. A. Wilson, B. Kaiser, W. Jaegermann, L. Francàs, S. Gimenez, J. R. Durrant, *Sustain. Energy Fuels* **2020**, *4*, 5024–5030.
[23] B. J. Taitt, D. H. Nam, K. S. Choi, *ACS Catal.* **2019**, *9*, 660–670.
[24] C. Wei, Z. J. Xu, C. Wei, Z. J. Xu, *Small Methods* **2018**, *2*, 1800168.
[25] A. Zülke, P. Perroni, E. G. Machado, H. Varela, *ECS Trans.* **2017**, *77*, 1643–1650.
[26] C. P. Oliveira, N. V. Lussari, E. Sitta, H. Varela, *Electrochim. Acta* **2012**, *85*, 674–679.
[27] G. Melle, M. B. C. de Souza, P. V. B. Santiago, P. G. Corradini, L. H. Mascaro, P. S. Fernández, E. Sitta, *Electrochim. Acta* **2021**, *398*, 139318.
[28] X. Shi, D. E. Simpson, D. Roy, *Phys. Chem. Chem. Phys.* **2015**, *17*, 11432–11444.
[29] S. Y. Jung, S. Kang, K. M. Kim, S. Mhin, J. C. Kim, S. J. Kim, E. Enkhtuvshin, S. Choi, H. S. Han, *Appl. Surf. Sci.* **2021**, *568*, 150965.
[30] T. E. Jones, R. Wyrwich, S. Böcklein, E. A. Carbonio, M. T. Greiner, A. Y. Klyushin, W. Moritz, A. Locatelli, T. O. Menteş, M. A. Niño, A. Knop-Gericke, R. Schlögl, S. Günther, J. Wintterlin, S. Piccinin, *ACS Catal.* **2018**, *8*, 3844–3852.
[31] Z. Li, M. Shao, H. An, Z. Wang, S. Xu, M. Wei, D. G. Evans, X. Duan, *Chem. Sci.* **2015**, *6*, 6624–6631.

Manuscript received: January 24, 2022
Revised manuscript received: March 14, 2022
Accepted manuscript online: March 31, 2022